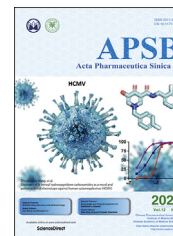




Chinese Pharmaceutical Association
Institute of Materia Medica, Chinese Academy of Medical Sciences

Acta Pharmaceutica Sinica B

www.elsevier.com/locate/apsb
www.sciencedirect.com



ORIGINAL ARTICLE

Discovery of *N*-benzyl hydroxypyridone carboxamides as a novel and potent antiviral chemotype against human cytomegalovirus (HCMV)



Sameera Senaweera^{a,†}, Tiffany C. Edwards^{a,†}, Jayakanth Kankanala^a, Yan Wang^{a,b}, Rajkumar Lalji Sahani^a, Jiashu Xie^a, Robert J. Geraghty^a, Zhengqiang Wang^{a,*}

^aCenter for Drug Design, College of Pharmacy, University of Minnesota, Minneapolis, MN 55455, USA

^bTranslational Medicine R&D Center, Shenzhen Institutes of Advanced Technology, Chinese Academy of Sciences, Shenzhen 518055, China

Received 25 June 2021; received in revised form 5 August 2021; accepted 17 August 2021

KEY WORDS

Human cytomegalovirus;
N-Benzyl
hydroxypyridone
carboxamides;
Structure–activity
relationship;
Mechanism of action

Abstract Current drugs for treating human cytomegalovirus (HCMV) infections are limited by resistance and treatment-associated toxicities. In developing mechanistically novel HCMV antivirals, we discovered an *N*-benzyl hydroxypyridone carboxamide antiviral hit (**8a**) inhibiting HCMV in submicromolar range. We describe herein the structure–activity relationship (SAR) for **8a**, and the characterization of potent analogs for cytotoxicity/cytostatic property, the preliminary mechanism of action, and the absorption, distribution, metabolism and excretion (ADME) properties. The SAR revealed a few pharmacophore features conferring optimal antiviral profile, including the 5-OH, the *N*-1 benzyl, at least one –CH₂– in the linker, and a di-halogen substituted phenyl ring in the amide moiety. In the end, we identified numerous analogs with sub-micromolar antiviral potency and good selectivity index. The preliminary mechanism of action characterization used a pUL89-C biochemical endonuclease assay, a virus entry assay, a time-of-addition assay, and a compound withdrawal assay. ADME profiling measuring aqueous solubility, plasma and liver microsomal stability, and parallel artificial membrane permeability assay (PAMPA) permeability demonstrated largely favorable drug-like properties. Together, these studies validate the *N*-benzyl hydroxypyridone carboxamide as a viable chemotype for potent and mechanistically distinct antivirals against HCMV.

*Corresponding author. Tel.: +1 612 6267025.

E-mail address: wangx472@umn.edu (Zhengqiang Wang).

[†]These authors made equal contributions to this work.

Peer review under responsibility of Chinese Pharmaceutical Association and Institute of Materia Medica, Chinese Academy of Medical Sciences.

<https://doi.org/10.1016/j.apsb.2021.08.019>

2211-3835 © 2022 Chinese Pharmaceutical Association and Institute of Materia Medica, Chinese Academy of Medical Sciences. Production and hosting by Elsevier B.V. This is an open access article under the CC BY-NC-ND license (<http://creativecommons.org/licenses/by-nc-nd/4.0/>).

1. Introduction

Human cytomegalovirus (HCMV) is a highly prevalent beta-herpesvirus¹. Although typically asymptomatic with immunocompetent persons, HCMV infections can be dangerous to individuals with compromised or immature immune systems². Importantly, congenital HCMV infection leads to permanent neurological defects in infants with a range of severe symptoms³. In addition, HCMV also causes significant morbidity and mortality to immunocompromised individuals, such as HIV-1 infected patients⁴ and organ transplant recipients⁵. Until recently, treatment of HCMV infections has relied solely on viral polymerase inhibitors⁶ (Fig. 1, 1–3), particularly ganciclovir (GCV, 1), the drug choice for treatment^{7,8} and prophylaxis⁹. However, ganciclovir produces only modest efficacy while exhibiting dose-limiting toxicities, resulting in drug resistance and treatment failure^{10,11}. Two additional polymerase inhibitors, cidofovir (2), and foscarnet (3), have been in use as secondary therapies, though both also suffer from toxicities and resistance¹². The only non-polymerase targeting HCMV drug is the recently FDA-approved letermovir¹³ (Fig. 1, 4) which uniquely inhibits the viral terminase complex¹⁴, presumably by targeting pUL56^{15,16}, a noncatalytic guide protein. The approval of letermovir provides a strong clinical validation for targeting viral terminase complex for developing new HCMV antiviral drugs^{17,18}.

We have been interested in inhibiting the terminase complex by targeting the catalytic protein pUL89, specifically the metal-dependent endonuclease activity located at the C terminus (pUL89-C)^{19–21}. Due to a high degree of similarities among pUL89-C, HIV-1 integrase and RNase H in active site fold and catalytic mechanism^{22,23}, our medicinal chemistry approach is

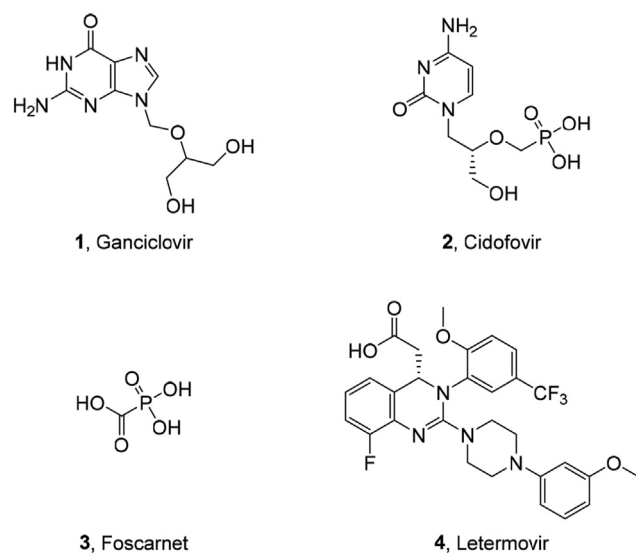


Figure 1 Structures of FDA-approved HCMV drugs. Ganciclovir (1), cidofovir (2), foscarnet (3) target viral polymerase, whereas letermovir (4) targets viral terminase complex.

based on metal-binding small molecules. To that end, we have identified and characterized hydroxypyridine carboxylic acid (HPCA) as the first pUL89-C inhibitor type (5, Fig. 2A)^{19,21}. Interestingly, while the prototypical HPCA 5 inhibited both HCMV and pUL89-C in low $\mu\text{mol/L}$ range, converting the acid into ester (6) or carboxamide (7) led to significant potency reduction against pUL89-C²¹ (Fig. 2A), presumably due to alterations in electronic properties around the chelating triad. More dramatically, introducing an *N*-di-fluorobenzyl group onto the carboxamide resulted in a compound (8a) with substantially improved antiviral activity ($\text{EC}_{50} = 0.86 \mu\text{mol/L}$ for 8a vs. $\text{EC}_{50} = 10 \mu\text{mol/L}$ for 5), but essentially no inhibition against pUL89-C (Fig. 2A).

The lack of pUL89-C inhibition by 8a was corroborated by the molecular modeling (Fig. 2B and C). When docked into the pUL89-C active site (PDB code: 6EY7²⁴), the preferred conformation of HPCA analog 5 allowed three key binding interactions: the effective chelation with the two divalent metal ions, the salt-bridge between the carboxylic acid functional group and K583, and a critical π - π stacking between the phenyl ring on N-1 position and the phenyl ring of F466 (Fig. 2B). Collectively, these favorable interactions amount to an excellent docking score of -9.1 kcal/mol . In stark contrast, the bulky amide of 8a forced the compound to turn away from the preferred binding mode, resulting in the complete loss of the salt-bridge, π - π stacking interactions, and the triad metal chelation (Fig. 2C). The poor docking score of -4.9 kcal/mol for compound 8a theoretically predicts a pUL89-C inhibitory activity orders of magnitude lower than that of 5. Together, these observations strongly indicate that 8a represents a mechanistically novel HCMV antiviral hit and warrants further medicinal chemistry studies. We report herein the structure–activity relationship (SAR, Fig. 3), ADME profiling, and preliminary mechanistic characterization of this novel inhibitor type.

2. Results and discussion

2.1. Compound synthesis

The chemical synthesis of subtypes 8–15 all involved a pyridone carboxylate core (21–23, Scheme 1; and 31, Scheme 2), whereas subtypes 16–17 were synthesized *via* a pyranone carboxylate core (36, Scheme 3; and 41, Scheme 4). In general, the synthesis was adapted from our previously reported procedures²⁵. In a representative synthesis, commercially available, substituted methyl or ethyl acetoacetates were subjected to a one-carbon homologation to yield enamines (19, 35, and 40). The subsequent Claisen condensation followed by an immediate cyclization produced the pyrone intermediates 20, 36, and 41. The conversion of the pyranone ring into pyridone (21–23, 37 and 42) was effected *via* an amination with corresponding amines under thermal conditions. Resulting intermediates were then saponified to afford the pyridone carboxylic acid analogs (24–26, 32, 38, and 43) which were then subjected to HATU coupling to afford the corresponding amides (27–29, 33, 16, 17). Finally, *O*-debenzylation under catalytic hydrogenation conditions or using TFA produced the final products (8a–w, 9a–d, 10–15).

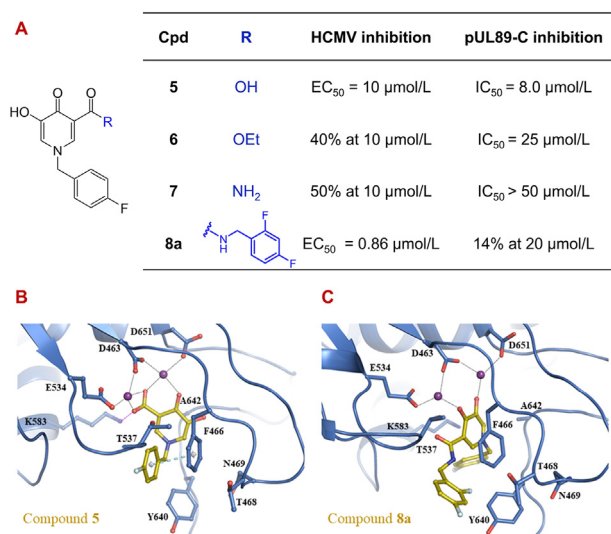


Figure 2 Identification of **8a** as an HCMV antiviral hit. (A) Compound **8a** potentially inhibited HCMV without inhibiting pUL89-C; (B) and (C) Predicted binding modes of the prototypical HPCA **5** (B) and the new antiviral hit **8a** (C) into the active site of pUL89-C (PDB code: 6EY7²⁴). Docking scores: -9.1 (**5**) and -4.9 kcal/mol (**8a**). Mn²⁺ ions, chelating triad, salt-bridge, and π - π stacking are depicted as violet spheres, black-, pink-, and cyan-dashed lines. The nitrogen, oxygen, and fluorine atoms are colored blue, red, and light green.

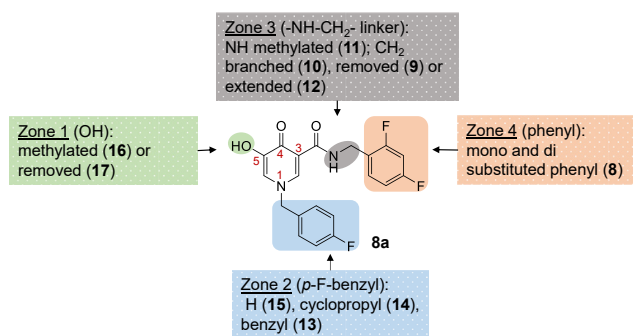


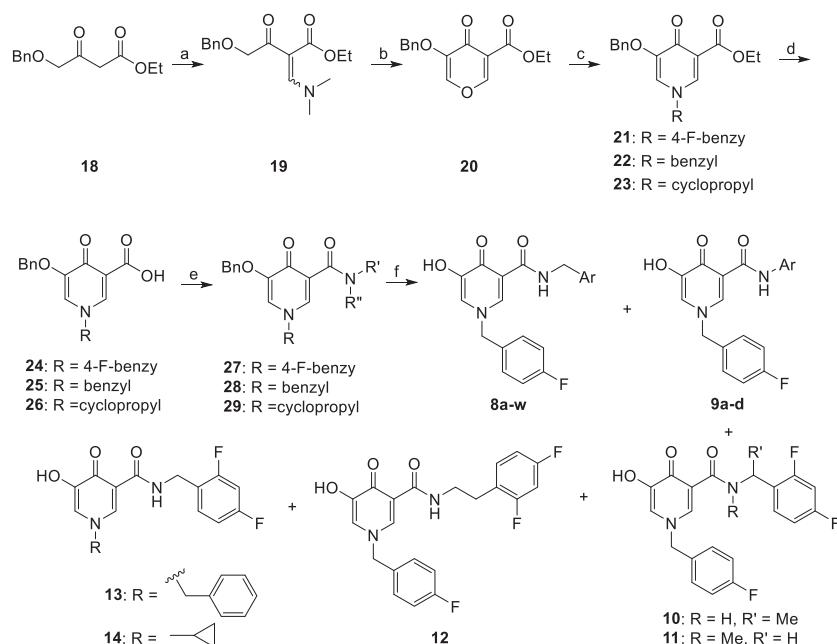
Figure 3 SAR plan for the HCMV antiviral hit **8a**. Four SAR zones are considered: zone 1 probes the 5-OH with subtypes **16**–**17**; zone 2 studies the N-1 substitution with subtypes **13**–**15**; zone 3 concerns the $-\text{NH}-\text{CH}_2-$ linkage with subtypes **9**–**12**; and zone 4 focuses on terminal phenyl ring with subtype **8**.

A slightly modified sequence was used for the synthesis of the N-unsubstituted subtype **15** (Scheme 2). This synthesis did not go through a pyranone intermediate. Instead, the dimethylenamine **19** was aminolysized using ammonium acetate *via* a conjugate addition followed by the elimination to produce enamine **30**. Cyclization of **30** followed by saponification yielded pyridone carboxylic acid **32**, which was converted to the amide **33** *via* HATU coupling. The final *O*-debenzylation under TFA afforded the final product **15**.

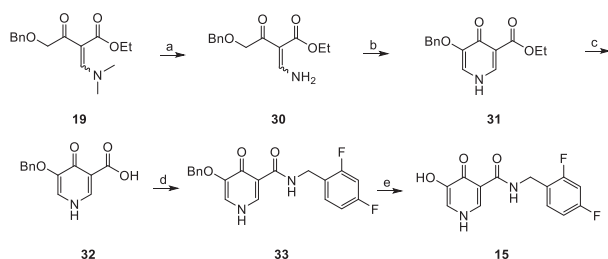
2.2. Structure–activity relationship (SAR)

The current SAR studies involved a total of 37 analogs probing four zones (Fig. 3), 23 of which belong to subtype **8** for SAR zone 4. Although these analogs were not expected to inhibit pUL89-C,

a single concentration (20 μmol/L) counter-screening was conducted using an ELISA-based biochemical endonuclease assay, from which only insignificant or marginal inhibition (3%–15%) was observed (Table 1), confirming that they do not target pUL89-C. The SAR was based on dose–response antiviral testing and the resulting EC₅₀ values. In addition, each compound was also tested in a parallel dose–response cytotoxicity assay, which allowed the calculation of a selectivity index (SI = CC₅₀/EC₅₀). These studies revealed the following SAR trends: 1) the 5-OH group is critical for potency. When this OH group was removed, the resulting analog (**17**) showed significantly reduced antiviral potency when compared to **8a** (EC₅₀ = 6.6 μmol/L for **17** vs. 0.86 μmol/L for **8a**). In a more dramatic fashion, methylating the 5-OH completely abrogated the antiviral potency (EC₅₀ > 50 μmol/L for **16**). Consistent with this observation, the two carboxylic acid precursors (**37** and **42**) produced no antiviral activity at concentrations up to 50 μmol/L (Table 1). 2) An N-1 benzyl group maximally benefits antiviral potency. As far as zone 2 is concerned, the N-1 unsubstituted analog (**15**, EC₅₀ = 8.0 μmol/L) and the N-1 cyclopropyl analog (**14**, EC₅₀ = 4.8 μmol/L) remained active, though the antiviral potency was considerably reduced when compared to hit **8a** (EC₅₀ = 0.86 μmol/L) bearing an N-1 *para*-F benzyl group. Removing the *para*-F group led to a slight decrease in antiviral potency (**13**, EC₅₀ = 1.0 μmol/L). These results indicate that an N-1 benzyl group confers optimal potency. 3) The $-\text{NH}-$ of the linkage (zone 3) was much less tolerant than the $-\text{CH}_2-$ toward modifications. When the $-\text{NH}-$ of the linkage was methylated, the resulting compound (**11**) conferred slightly reduced potency (EC₅₀ = 1.4 μmol/L) and significant cytotoxicity (CC₅₀ = 12 μmol/L), suggesting that the $-\text{NH}-$ should be kept intact. By contrast, when the $-\text{CH}_2-$ was branched (**10**, EC₅₀ = 0.53 μmol/L), extended (**12**, EC₅₀ = 0.43 μmol/L), or removed (**9a**, EC₅₀ = 0.46 μmol/L), the resulting analogs all showed improved potency over **8a** (EC₅₀ = 0.86 μmol/L). However, the analog with a shortened linkage (**9a**) displayed severe cytotoxicity (CC₅₀ = 2.5 μmol/L). This profile of increased activity and cytotoxicity was consistently observed with **9a** congeners **9b** (EC₅₀ = 0.87 μmol/L; CC₅₀ = 5.6 μmol/L) and **9d** (EC₅₀ = 0.78 μmol/L; CC₅₀ = 6.5 μmol/L). The only exception was analog **9c** where a *para*-borate functional group conferred decreased potency, but no cytotoxicity. Collectively, these observations suggest that the $-\text{CH}_2-$ from the linkage should not be removed. 4) Substitutions on the amide phenyl ring (zone 4) impacted antiviral potency. Much of the SAR for **8a** focused on fine tuning the antiviral profile *via* probing the effects of various substituents on the phenyl ring. For this purpose, a total of 23 analogs were synthesized, with the phenyl ring mono-, di- or tri-substituted with various functional groups, particularly halogens. Other functional groups explored include Me (**8s** and **8t**), CN (**8r**), CF₃ (**8u**), borate (**8c**), and a fused pyrrole (**8w**). Although the SAR was not steep (EC₅₀ = 0.3–2.3 μmol/L) in general (Table 1), analogs devoid of any halogen substituent, such as the unsubstituted **8d** (EC₅₀ = 1.5 μmol/L), the fused pyrrole **8w** (EC₅₀ = 1.6 μmol/L), and the borate substituted **8c** (EC₅₀ = 2.3 μmol/L); and those with a combination of one halogen and one non-halogen substituents, *e.g.*, **8r** (EC₅₀ = 1.2 μmol/L) and **8s** (EC₅₀ = 1.0 μmol/L), were less potent than analogs with halogen only substitutions. Among analogs with halogen only substituents, no discernible potency trend was observed with regard to specific halogens (F vs. Cl vs. Br), the multitude of substitution (mono vs. di vs. tri) or the substitution pattern (*para* vs. *meta* vs. *ortho*), with the exception of



Scheme 1 Synthesis of **8–14**. Reagents and conditions: a) DMF-DMA, 100 °C, MW, 75%; b) ethyl formate, KOrBu, THF, rt, 85%; c) R–NH₂, EtOH, 100 °C, 1 h, MW, 40%–85%; d) 2 mol/L NaOH, EtOH, 90 °C, 4–6 h, 65%–95%; e) R'R''NH, HATU, DIPEA, DMF, rt, 12 h, 72%–80%; f) H₂, Pd/C, MeOH, rt, 1 h, 60%–87%.



Scheme 2 Synthesis of **15**. Reagents and conditions: a) NH₄OAc, EtOH, reflux, 1 h, 86%; b) ethyl formate, KOrBu, THF, rt, 65%; c) 2 mol/L NaOH, EtOH, 90 °C, 4–6 h, 65%–95%; d) HATU, DIPEA, DMF, rt, 12 h, 72%–80%; e) TFA, 100 °C, 1 h, MW, 87%.

mono-F substitution, where significant difference was observed with *para*-F (**8b**, EC₅₀ = 0.78 μmol/L), *meta*-F (**8f**, EC₅₀ = 0.97 μmol/L) and *ortho*-F (**8e**, EC₅₀ = 1.6 μmol/L). Overall, di-halogen substitution appeared to confer the optimal antiviral potency.

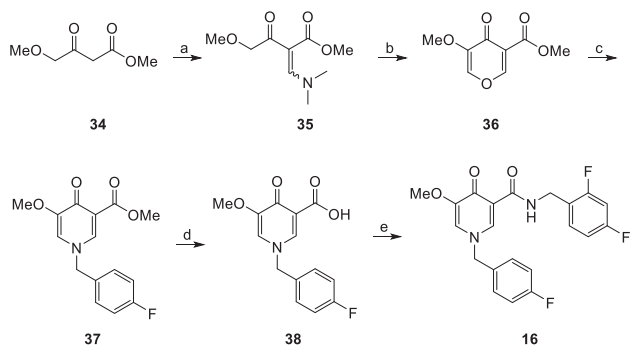
As far as cytotoxicity is concerned, many of these analogs showed cytotoxicity with CC₅₀ values in the low μmol/L range, though some of the compounds may inhibit cell growth (cytostatic) instead of killing the cells (cytotoxic). An example is **8p** where there was little dose–response when the compound was examined for effects on cell viability over concentrations 0.2–50 μmol/L (Fig. 4B). The MTS assay showed approximately 50% metabolic activity across all compound concentrations of **8p** compared to DMSO yet when examined by trypan blue exclusion, cells treated with 10 or 50 μmol/L compound **8p** were >90% viable (data not shown). Therefore, **8p** appears to cause a cytostatic but not a cytotoxic effect. Further studies exploring this property of **8p** are currently underway.

Overall, our studies identified a total of eight *N*-benzyl hydroxypyridone carboxamide analogs potentially inhibiting HCMV with antiviral EC₅₀s ≤ 1.0 μmol/L (Table 2). In addition, although reduction in cell viability was observed as compared to DMSO control, the reduction plateaued at around 50% at high concentrations (up to 50 μmol/L), amounting to large CC₅₀ values and selectivity indices (Table 2). Curves from dose–response antiviral (A) and viability (B) assays for representative antiviral (**8p**, **12**, **13**, and the control compound GCV (**1**)) are shown in Fig. 4.

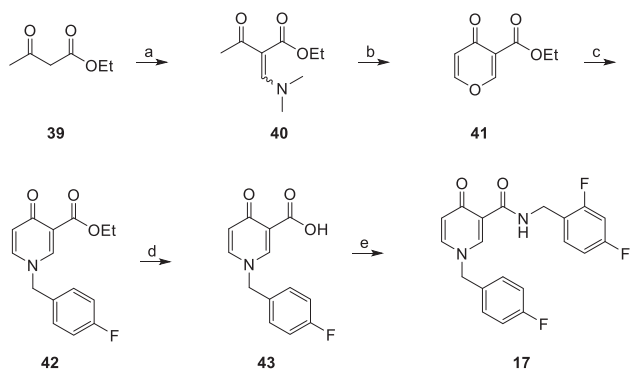
2.3. Preliminary antiviral mechanism of action

To begin characterizing the mechanism of action for the *N*-benzyl hydroxypyridone carboxamides, we conducted experiments aiming to determine when the compounds act during viral replication. To determine if the compounds inhibit viral entry, HFF cells were dosed with 5 × EC₅₀ of test compounds or 10 μg/mL heparin at different times as shown in Fig. 5A. HFFs were inoculated with HCMV ADCREGFP reporter virus at a multiplicity of infection (MOI) of 0.01 and cultured for 168 h before lysis and relative GFP intensity was determined. If the compounds inhibit HCMV entry by binding to an important cellular receptor, we expect that pre-treating the cells would prevent viral absorption. If the compounds inhibit HCMV by binding to viral surface glycoproteins to prevent entry, the compounds will block infection when they are present during the initial viral inoculation. Heparin (10 μg/mL), a known entry inhibitor that binds viral surface proteins to prevent virus attachment to the cell, inhibited viral absorption only when the compound was added during entry (Fig. 5B). Compounds **12** and **13** and the polymerase inhibitor GCV did not inhibit HCMV unless they were added and maintained after the initial infection (Fig. 5B), indicating they do not block virus entry.

Time-of-addition (TOA)^{26,27} studies are commonly used to determine when a compound acts during viral replication. A



Scheme 3 Synthesis of **16**. Reagents and conditions: a) DMF-DMA, 100 °C, MW, 70%; b) ethyl formate, KOtBu, THF, rt, 72%; c) R-NH₂, EtOH, 100 °C, 1 h, MW, 40%–85%; d) 2 mol/L NaOH, EtOH, 90 °C, 4–6 h, 65%–95%; e) amine, HATU, DIPEA, DMF, rt, 12 h, 80%.



Scheme 4 Synthesis of **17**. Reagents and conditions: a) DMF-DMA, 100 °C. MW, 67%; b) ethyl formate, KOtBu, THF, rt, 80%; c) R-NH₂, EtOH, 100 °C, 1 h, MW, 40%–85%; d) 2 mol/L NaOH, EtOH, 90 °C, 4–6 h, 65%–95%; e) R'R''NH, HATU, DIPEA, DMF, rt, 12 h, 72%–80%.

compound can only block viral replication if it inhibits its target before the target's role in replication. To elucidate the earliest point during HCMV replication the compounds are active, HFF cells were inoculated with HCMV ADCREGFP at an MOI of 0.01 for 2 h and then treated with compounds at $5 \times$ the EC₅₀ at the indicated time points (Fig. 5C). In this study two control compounds, GCV (polymerase inhibitor) and LTV (terminase inhibitor), were used because they inhibit different steps during viral replication. GCV acts post-entry to block viral genome synthesis and before LTV blocks genome cleavage during genome packaging, a relatively late step in virus replication. As expected, GCV lost significant inhibitory activity when added after 48 h post infection and LTV remained effective when added before 72 h post infection. Compound **12** appeared to inhibit viral replication at a stage between when GCV and LTV are active, while compound **13** appeared to be active similar to, or possibly later than, LTV (Fig. 5D). These data seemed to indicate that the two structurally similar compounds act at different time points during viral replication.

To confirm the TOA data, we carried out a compound withdrawal assay. In this assay, infected cells treated with late-stage inhibitors like LTV will have a rapid recovery of viral replication

when compound is removed. In comparison, infected cells treated with GCV will have a delayed recovery of viral replication when compound is removed because GCV acts relatively early compared to LTV. HFFs were inoculated with HCMV ADCREGFP at an MOI of 0.01 for 2 h and the cells were treated with compound at $5 \times$ EC₅₀. Compound was removed at the indicated time points (Fig. 5E) and viral replication was allowed to proceed until 168 h post infection when the cells were lysed and GFP fluorescence intensity measured. As expected, when LTV was removed, the viral infection rebounded quickly compared to GCV which acts earlier during viral replication. Consistent with the time of addition studies, compound **12** appeared to inhibit a step in viral replication between LTV and GCV. Interestingly, when compound **13** was withdrawn viral replication recovered similarly to GCV (Fig. 5F) suggesting that the compound acts early during viral replication, in direct contrast to the time of addition assay (Fig. 5D).

While these data do not definitively tell us when the compounds are active during viral replication, they provide clues to follow up on in a later study. We hypothesize that the compounds may inhibit more than one viral and/or cellular target or inhibit a target that is critical at more than one stage during viral replication.

2.4. ADME profiling

To evaluate the drug-like properties of the novel N-benzyl hydroxypyridone carboxamide HCMV inhibitor type, two selected analogs, **12** and **13**, were tested in our ADME assays to measure aqueous solubility, plasma stability, microsomal stability and PAMPA permeability (Table 3). Both analogs exhibited excellent plasma stability, good microsomal stability, and high permeability, predicting largely favorable bioavailability. The only ADME weakness for **12** and **13** was the low thermodynamic aqueous solubility, though this concern is partially mitigated by their high permeability, as the required solubility is inversely proportional to permeability^{28,29}.

3. Conclusions

During our SAR studies on the HPCA inhibitor type **5** of HCMV pUL89-C, a structurally more elaborate N-benzyl carboxamide subtype **8a** produced markedly enhanced antiviral potency over **5** but virtually no pUL89-C inhibition. In the current work, we have designed and synthesized a total of 37 analogs to probe four SAR zones of **8a**. The SAR was based on the EC₅₀ values from the dose–response antiviral testing. Cytotoxicity was also included in the antiviral profiling. These studies uncovered a several important SAR trends, which collectively identified a few pharmacophore features favoring the optimal antiviral profile, including the 5-OH, the N-1 benzyl, at least one –CH₂– in the linker, and the dihalogen substituted phenyl ring in the amide moiety. Importantly, many analogs demonstrated potent antiviral activities (EC₅₀ ≤ 1.0 μmol/L) and no cytotoxicity (CC₅₀ > 50 μmol/L). The lack of pUL89-C inhibition by these compounds was confirmed in a biochemical endonuclease assay. Further MOA studies using virus entry, TOA and compound withdrawal assays demonstrated a complicated post-entry inhibition pattern indicating these compounds may inhibit more than one viral and/or cellular target or one target that acts at more than one stage during virus replication. ADME profiling by measuring aqueous

Table 1 Dose–response antiviral EC₅₀, cell viability CC₅₀, and the single-dose inhibition % in the endonuclease assay for the *N*-benzyl hydroxypyridone carboxamides.

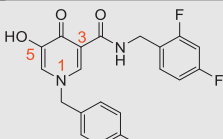
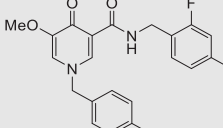
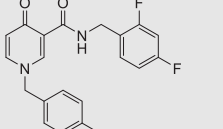
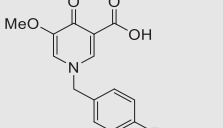
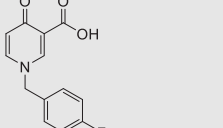
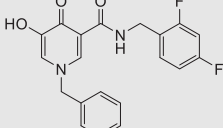
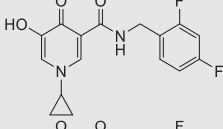
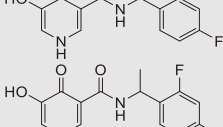
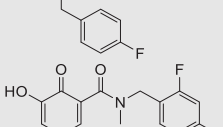
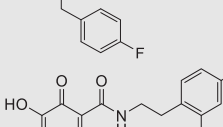
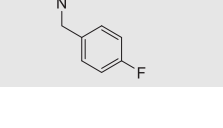
Compd.	Structure	Endonuclease inhibition (%) at 20 μmol/L	Cell-based assay		
			EC ₅₀ ^a (μmol/L)	CC ₅₀ ^b (μmol/L)	SI ^c
8a		14	0.86 ± 0.14	>50	>58
16		6	>50	>50	—
17		5	6.6 ± 0.7	>50	>7.6
37		8	>50	>50	—
42		7	>50	>50	—
13		6	1.0 ± 0.11	>50	>50
14		7	4.8 ± 0.25	>25	>5.2
15		7	8.0 ± 0.1	>50	>6.3
10		5	0.53 ± 0.09	>50	>94
11		6	1.4 ± 0.05	12 ± 4.9	8.6
12		10	0.43 ± 0.12	>50	>116

Table 1 (continued)

Compd.	Structure	Endonuclease inhibition (%) at 20 $\mu\text{mol/L}$	Cell-based assay		
			EC ₅₀ ^a ($\mu\text{mol/L}$)	CC ₅₀ ^b ($\mu\text{mol/L}$)	SI ^c
9a		13	0.46 \pm 0.08	2.5 \pm 0.2	5.4
9b		9	0.87 \pm 0.01	5.6 \pm 1.3	6.4
9c		7	3.0 \pm 0.1	>50	>17
9d		7	0.78 \pm 0.23	6.5 \pm 2.4	8.3
8b		7	0.78 \pm 0.06	6.4 \pm 3.7	8.2
8c		5	2.3 \pm 0.05	>50	22
8d		9	1.5 \pm 0.45	7.1 \pm 6.4	4.7
8e		6	1.6 \pm 0.4	5.8 \pm 2.1	3.6
8f		7	0.97 \pm 0.14	3.9 \pm 1.8	4.0
8g		7	0.74 \pm 0.04	17 \pm 3.7	23

(continued on next page)

Table 1 (continued)

Compd.	Structure	Endonuclease inhibition (%) at 20 $\mu\text{mol/L}$	Cell-based assay		
			EC ₅₀ ^a ($\mu\text{mol/L}$)	CC ₅₀ ^b ($\mu\text{mol/L}$)	SI ^c
8h		8	0.67 \pm 0.2	13 \pm 12	19
8i		6	0.60 \pm 0.15	7.5 \pm 2.3	13
8j		6	1.4 \pm 0.05	>50	36
8k		14	0.55 \pm 0.0	2.4 \pm 0.07	4.4
8l		14	0.48 \pm 0.03	>50	>104
8m		15	0.41 \pm 0.02	3.7 \pm 1.9	9.0
8n		5	0.62 \pm 0.12	3.9 \pm 2.3	6.3
8o		7	0.7 \pm 0.19	5.3 \pm 2.1	7.6
8p		5	0.30 \pm 0.02	NC ^d	—
8q		9	0.61 \pm 0.13	>25	>41
8r		5	1.2 \pm 0.05	>50	>42

Table 1 (continued)

Compd.	Structure	Endonuclease inhibition (%) at 20 $\mu\text{mol/L}$	Cell-based assay		
			EC ₅₀ ^a ($\mu\text{mol/L}$)	CC ₅₀ ^b ($\mu\text{mol/L}$)	SI ^c
8s		6	1.0 \pm 0.07	10 \pm 5.4	10
8t		8	0.98 \pm 0.03	>50	>51
8u		3	0.54 \pm 0.05	>25	>46
8v		5	0.7 \pm 0.27	5.7 \pm 2.0	8.1
8w		14	1.6 \pm 0.2	12 \pm 12	7.5
1	—	—	1.0 \pm 0.12	>50	>50

^aEC₅₀: concentration of compound inhibiting HCMV replication by 50%, expressed as the mean \pm SD from at least two independent experiments.

^bCC₅₀: concentration of compound causing 50% cell death, expressed as the mean \pm SD from at least two independent experiments.

^cSI: selectivity index, defined as CC₅₀/EC₅₀.

^dNC: not calculable. No CC₅₀ could be calculated due to the lack of a dose–response.

solubility, plasma and liver microsomal stability and PAMPA permeability with two selected analogs showed generally favorable drug-like properties. Collectively, these results validate the N-benzyl hydroxypyridone carboxamide chemotype as a novel platform for developing potent and mechanistically distinct antivirals against HCMV.

4. Experimental

4.1. Chemistry

4.1.1. General procedures

All commercial chemicals were used as supplied unless otherwise indicated. Flash chromatography was performed on a Teledyne Combiflash RF-200 with RediSep columns (silica) and indicated mobile phase. All moisture sensitive reactions were performed under an inert atmosphere of ultra-pure argon with oven-dried glassware. ¹H and ¹³C NMR spectra were recorded on a Varian 600 or Bruker 400 MHz spectrometers. Mass data were acquired using an Agilent 6230 TOF LC/MS spectrometer. See supplementary materials for detailed synthetic procedure, compound characterization data and original ¹H and ¹³C NMR spectra.

4.2. In vitro pUL89-C endonuclease assay

pUL89-C was expressed in bacteria and purified as previously described¹⁹. A 60-bp ssDNA with a 5' digoxigenin (DIG) tag (5'-taatcgccctgcagcacatcccccttcgacgctggcgtaatagcgaagagcccgac) was annealed to a complementary 60-bp ssDNA with a 5' biotin tag (5'-tcggctgcggcctcttcgctattaccgacgctggcgaaggggatgtgctg-caaggcga) (IDT) to form a 60-bp dsDNA substrate by mixing equimolar amounts of each ssDNA. Twenty $\mu\text{mol/L}$ of test compound was preincubated with 10 $\mu\text{mol/L}$ pUL89-C in reaction buffer (3 mmol/L MnCl₂, 30 mmol/L Tris pH 8 and 50 mmol/L NaCl) for 15 min at room temperature. The dsDNA substrate (100 $\mu\text{mol/L}$ final concentration) was added to initiate the reaction. The reaction was incubated for 30 min at 37 °C and terminated by adding 10 μL of 0.5 mol/L EDTA. Samples were transferred to streptavidin coated plates (Pierce Biotechnology) and the dsDNA was allowed to bind for 30 min with rocking at room temperature. Samples were removed and the plate washed three times with 200 μL of wash buffer (25 mmol/L Tris, 150 mmol/L NaCl, 0.1% BSA, and 0.05% Tween-20; pH 7.2). The anti-DIG-alkaline phosphatase (AP) conjugate antibody (Roche Applied Sciences, Germany) was diluted to 0.15 U/mL and 100 μL of the diluted antibody added to each well. The plates

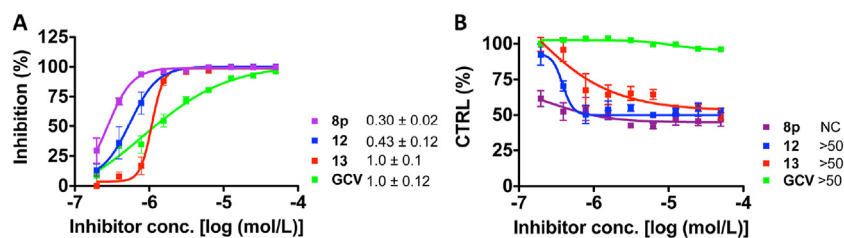


Figure 4 Dose–response analysis for HCMV inhibition and cell viability for selected compounds. (A) HFFs were inoculated with HCMV ADCREGFP and cultured in various compound doses for 168 h. Cells were lysed and relative fluorescence compared to that for DMSO control to calculate inhibition (%). Dose–response curves and EC_{50} values obtained using GraphPad Prism. (B) HFFs were treated with various compound doses in the absence of virus for 168 h. Cell viability was determined using an MTS assay. The viability (%) was determined by comparing to DMSO-treated control cultures. Dose–response curves and CC_{50} values obtained using GraphPad Prism. Data shown are the mean and standard deviations of three technical replicates. Each assay was repeated at least twice with representative curves shown. CTRL (%), percent of control.

Table 2 Summary of antiviral and cytotoxicity profiles of selected *N*-benzyl hydroxypyridone carboxamide analogs.

Compd.	EC_{50}^a ($\mu\text{mol/L}$)	CC_{50}^b ($\mu\text{mol/L}$)	SI ^c
8a	0.86 ± 0.14	>50	>58
8l	0.48 ± 0.03	>50	>104
8p	0.30 ± 0.02	NC ^d	–
8t	0.98 ± 0.03	>50	>51
8u	0.54 ± 0.05	>25	>46
10	0.53 ± 0.09	>50	>94
12	0.43 ± 0.12	>50	>116
13	1.0 ± 0.11	>50	>50

^a EC_{50} : concentration of compound inhibiting HCMV replication by 50%, expressed as the mean \pm SD from at least two independent experiments.

^b CC_{50} : concentration of compound causing 50% cell death, expressed as the mean \pm SD from at least two independent experiments.

^cSI: selectivity index, defined as CC_{50}/EC_{50} .

^dNC: not calculable. Viability around 50% at 50 $\mu\text{mol/L}$.

were incubated at room temperature with rocking for 30 min then washed three times with 200 μL of wash buffer. One hundred μL of *p*-nitrophenylphosphate (pNPP) (1 mg/mL, Sigma–Aldrich) was added to each well and the plate was incubated at room temperature for up to 30 min. The absorbance at 405 nm was read using a BioTek Neo 2 plate reader.

4.3. HCMV replication assay

HFF cells (ATCC#: CRL-2088) were grown in DMEM supplemented with 10% FBS and 1% penicillin streptomycin for up to 8 passages after thaw from liquid nitrogen. For HCMV replication inhibition assays, 1.75×10^4 cells/well were seeded onto low evaporation, clear 96-well tissue culture plates (ThermoFisher) and grown overnight at 37 °C in 5% CO₂. Twenty-four hours later, the HFFs were inoculated with HCMV ADCREGFP³⁰ (obtained from Wade Bresnahan, University of Minnesota) at a multiplicity of infection (MOI) of 0.01. After inoculation, the cells were cultured in DMEM with 5% FBS for the remainder of the assay. The viral inoculum was removed after 2 h at 37 °C and 100 μL /well phosphate-buffered saline (PBS) was used added and removed. One hundred μL of fresh media with test compounds dissolved in DMSO (0.5% DMSO final concentration) or 0.5% DMSO vehicle control was added the cultures. After 168 h, the

cells were lysed in 200 μL of lysis buffer [25 mmol/L Tris (pH 7.8)], 2 mmol/L dithiothreitol (DTT), 2 mmol/L *trans*-1,2-diaminocyclohexane-*N,N,N',N'*-tetraacetic acid, 1% Triton X-100, 10% glycerol] to measure fluorescence of the GFP produced from the viral genome. Cells were incubated with lysis buffer for 10 min at 37 °C followed by a 30 min incubation at room temperature with rocking. GFP relative fluorescence units were determined at excitation/emission 495/515 nm using a BioTek Neo2 plate reader. All compounds and controls were evaluated using triplicate wells and mean values were determined and compared to the mean value for the wells that received only the DMSO vehicle control. The normalized data was plotted using GraphPad Prism to determine the compound concentration resulting in a 50% reduction (EC_{50}) in virus replication (GFP fluorescence) compared to DMSO.

4.4. Cell viability assay

Cell viability assays were performed under identical conditions to the HCMV replication inhibition assays in the absence of virus. Briefly, 1.75×10^4 cells/well were seeded onto a low evaporation 96 well tissue culture dish and grown overnight. Twenty-four hours later test compounds were applied to cells in DMEM with 5% FBS and 1% P/S. HFFs were incubated with test compounds for 168 h at 37 °C in 5% CO₂. Cellular viability was determined using CellTiter 96 Aqueous Non-Radioactive cell proliferation assay (Promega) according to the manufacturer's instructions. Each compound was tested in triplicate and the mean value for each compound was determined. The mean value of the test compound was compared to the mean value for the wells that received DMSO alone. The 50% cytotoxic concentration (CC_{50}) was determined using Graph Pad Prism software.

4.5. Virus entry assay

HFFs were seeded onto 96-well tissue culture dishes at 1.75×10^4 cells/well. The following day, the media was retired and replaced with media containing test compounds, heparin, or 0.5% DMSO 2 h before virus inoculation and then removed prior to inoculation, 2 h before inoculation and maintained throughout inoculation, only during the inoculation, or after inoculation. All test compounds were applied at $5 \times EC_{50}$ (Table 1) and heparin at 10 $\mu\text{g}/\text{mL}$ as a control compound to inhibit HCMV entry by blocking viral uptake³¹. For virus inoculation, the media was retired, cells were washed in 100 $\mu\text{L}/\text{well}$ PBS and inoculated with HCMV ADCREGFP at an MOI of 0.01 with or without test and

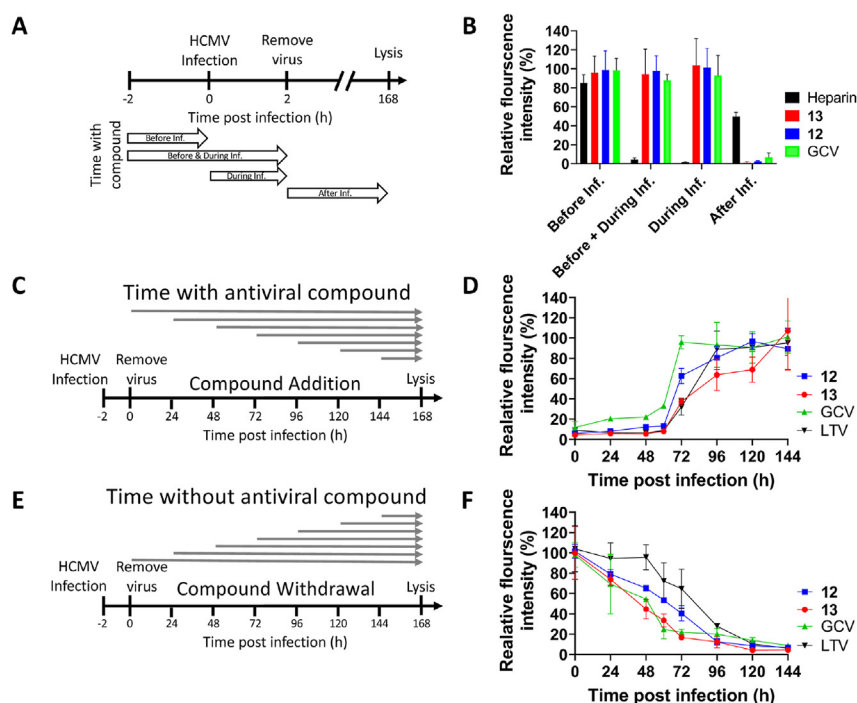


Figure 5 Preliminary analysis of **12** and **13** mechanism of action against HCMV: (A) Schematic representation of viral entry assay. (B) Representative viral entry inhibition assay data by representative compounds with relative fluorescence intensity compared to that from DMSO measuring GFP produced by HCMV reporter virus. Compounds at $5 \times EC_{50}$ or $10 \mu\text{g/mL}$ (heparin) were added at times indicated. (C) Schematic representation of the time of addition assay. (D) Representative time of addition assay data with Relative fluorescence intensity compared to that from DMSO measuring GFP produced by HCMV reporter virus. Compound final concentrations were $5 \times EC_{50}$. (E) Schematic representation of the compound withdrawal assay. (F) Representative compound withdrawal assay data with Relative fluorescence intensity compared to that from DMSO measuring GFP produced by HCMV reporter virus. Compound final concentrations were $5 \times EC_{50}$. All data shown is the mean and standard deviation of three technical replicates. Each assay was repeated at least twice.

Table 3 Solubility, permeability and *in vitro* metabolic stabilities of analogs **12** and **13**.

Compd.	Aqueous solubility ($\mu\text{mol/L}$) ^a , $n = 3$	Plasma stability $t_{1/2}$ (h), $n = 3$		Microsomal stability ^b $t_{1/2}$ (min), $n = 3$		PAMPA permeability P_c^c (10^{-6} cm/s), $n = 6$
		Human	Mouse	Human	Mouse	
12	2.2 ± 0.2	>24	>24	40.1 ± 1.8	26.0 ± 1.0	4.5 ± 0.9
13	2.2 ± 0.1	>24	>24	102.3 ± 11.8	53.7 ± 0.4	9.1 ± 1.1

Data are presented as mean \pm SD.

^aAqueous solubility were determined in Dulbecco's Phosphate-Buffered Saline (DPBS, pH 7.2).

^bCYP enzyme cofactor: NADPH.

^c P_c : the apparent permeability coefficient. High permeability: $>1.5 \times 10^{-6}$ cm/s; Low permeability: $<1.5 \times 10^{-6}$ cm/s.

control compounds in DMEM with 5% FBS, 1% P/S, and 0.5% DMSO. The viral inoculum was allowed to remain on the cells for 2 h at 37°C prior to removal and washing in PBS. Fresh media with or without test and control compounds was added to each well and the cells were cultured for 168 h. HCMV replication was assessed as described above.

4.6. Time of addition assay

Time of addition studies were performed as previously described¹⁹ with minor modifications. HFFs were seeded onto 96-well tissue culture dishes at 1.75×10^4 cells/well and cultured for 24 h in DMEM with 10% FBS and 1% P/S. Cells were inoculated with HCMV ADCREGFP at an MOI of 0.01 as described above. After

viral inoculation, cells were maintained in DMEM with 5% FBS, 1% P/S, and 0.5% DMSO until test compounds were applied at $5 \times EC_{50}$ at the indicated time points. To assess the level of viral replication the cells were lysed as described above and the GFP intensity was determined. The relative GFP intensity of each sample was determined and the mean for triplicate wells was calculated. All samples were normalized to DMSO.

4.7. Compound withdrawal assays

Compound withdraw studies were set up under identical conditions to the HCMV replication assays as described above. Cells were inoculated with HCMV ADCREGFP at an MOI of 0.01 for 2-h prior to compound addition. Test compounds were applied to

cells at $5 \times EC_{50}$ or 0.5% DMSO. Test compounds were removed at the indicated times and the cells were washed $2 \times$ in PBS (100 μ L/well) to remove any residual compound. Fresh media with 0.5% DMSO was added to each well after removal of compound. Cells were cultured for 168 h prior to lysis and GFP determination (described above). The relative GFP intensity of each sample was determined and the mean for triplicate wells was calculated. All samples were normalized to DMSO.

4.8. Aqueous solubility assay

To determine the aqueous solubility of each selected compound, a suspension was made by adding the Dulbecco's Phosphate-Buffered Saline (DPBS) to the solid compound. The suspension was shaken at 200 rpm for 72 h at ambient temperature to allow equilibrium between the solid and dissolved compound. A 0.45 μ m PVDF syringe filter was then used to remove the undissolved compound in DPBS. The filtrate was collected and analyzed immediately using an LC/MS/MS system consisting of an Agilent 1260 Infinity HPLC (Agilent Technologie, Santa Clara, CA, USA) and an AB Sciex QTrap 5500 mass spectrometer (AB Sciex LLC., Toronto, Canada).

4.9. Plasma stability assay

To determine the plasma stability, each selected compound (1 μ mol/L final concentration) was incubated in normal mouse (CD-1) or human plasma (Innovative Research, Novi, MI, USA) diluted to 80% with 0.1 mol/L potassium phosphate buffer (pH 7.4) at 37 °C. At various time points (up to 23 h), a 50 μ L aliquot of the plasma mixture was taken and quenched with 150 μ L of acetonitrile containing 0.1% formic acid. The quenched samples were then vortexed and centrifuged at 15,000 rpm (Eppendorf centrifuge 5424R, Enfield, CT, USA) for 5 min at 4 °C. The collected supernatants were analyzed by LC/MS/MS to determine the remaining percentages and *in vitro* plasma half-life ($t_{1/2}$) of the compound.

4.10. Microsomal stability assay

To determine the microsomal stability, each selected compound was incubated in commercially available liver microsomes of CD-1 mouse or human (Sekisui XenoTech, Kansas City, KS, USA) at 37 °C. Briefly, the selected compound (1 μ mol/L final concentration) was spiked into the reaction mixture containing liver microsomal protein (0.5 mg/mL final concentration) and $MgCl_2$ (1 mmol/L final concentration) in 0.1 mol/L potassium phosphate buffer (pH 7.4). The enzyme cofactor nicotinamide adenine dinucleotide phosphate (NADPH, 1 mmol/L final concentration) was then added to initiate the reaction. A negative control was performed in parallel without NADPH to reveal any chemical instability or non-NADPH dependent enzymatic degradation for each compound. Reaction with positive controls verapamil was also performed to confirm the proper functionality of the incubation system. At various time points (up to 60 min), a 50 μ L of reaction aliquot was taken and quenched with 150 μ L of acetonitrile containing 0.1% formic acid. The quenched samples were then vortexed and centrifuged at 15,000 rpm for 5 min at 4 °C. The collected supernatants were analyzed by LC/MS/MS to determine the *in vitro* metabolic half-life ($t_{1/2}$).

4.11. Parallel artificial membrane permeability assay (PAMPA)

The membrane permeability of selected compounds was evaluated in the Corning® BioCoat™ Pre-coated PAMPA Plate System (catalog. No. 353015, Corning, Glendale, AZ, USA) according to the manufacturer's protocol. Briefly, the thawed 96-well filter plate, pre-coated with lipids, was used as the permeation acceptor and a matching 96 well receiver plate was used as the permeation donor. The selected compounds were individually added to the wells (300 μ L/well) of the receiver plate in DPBS at a concentration of 2 μ mol/L. Blank DPBS was added to the wells (200 μ L/well) of the pre-coated filter plate. The plate assembly was then incubated at 25 °C without agitation for 5 h. At the end of the incubation, the plate assembly was disassembled and the final concentrations of compounds in both donor wells and acceptor wells were analyzed using LC/MS/MS. Permeability of the compounds were calculated using Eq. (1):

$$P_e = (-\ln[1 - C_a(t) / C_{eq}]) / (A \times (1 / V_d + 1 / V_a) \times t) \quad (1)$$

where A = filter area (0.3 cm²), V_d = donor well volume (0.3 mL), V_a = acceptor well volume (0.2 mL), t = incubation time (s), $C_a(t)$ = compound concentration in acceptor well at time t , $C_d(t)$ = compound concentration in donor well at time t , and C_{eq} was calculated using Eq. (2):

$$C_{eq} = [C_d(t) \times V_d + C_a(t) \times V_a] / (V_d + V_a) \quad (2)$$

A cutoff criteria of P_e value at 1.5×10^{-6} cm/s was used to classify the compounds into high and low permeability according to the literature report of this PAMPA plate system³².

4.12. Modeling and docking analysis

The binding of the key compounds to pUL89-C was evaluated *via* molecular modeling experiments using the Schrödinger small molecule drug discovery suite 2019-4³³. To perform these docking experiments, an HCMV terminase pUL89 nuclease domain in complex with gamma-diketoacid inhibitor was used (PDB code: 6EY7). Briefly, the tetrameric catalytic protein was first subjected to protein preparation and receptor grid generation, followed by ligand preparation of the key compounds, and finally docking of these compounds using Maestro³⁴ (Schrödinger; LLC: New York, NY, USA). First, protein preparation wizard³⁵ (Schrödinger; LLC: New York, NY, USA) was used to add zero-order bonds to metals, missing hydrogen atoms, side-chains, and loops onto the tetrameric protein. Afterwards, chain B, C, and D and waters beyond 5 Å were deleted; remaining water molecules inside the active site were manually deleted. To optimize the hydrogen bonding network and converge the heavy atoms to an RMSD of 0.3 Å, the prepared monomer protein was minimized using the OPLS3e force field³⁶. Next, the receptor grid generation tool in Maestro was used to define the active site around the native ligand gamma-diketoacid covering all the residues within 12 Å with both the metal cofactors (Mn^{2+}) as constraints to identify the chelating triad during docking. Prior to ligand docking, 2D-structure of each ligand was converted to low energy 3D-structure by subjecting to LigPrep that generate conformers, possible protonation at pH of 7 ± 2 , and metal binding states. Finally, all the compounds were docked using Glide XP³⁷ (Glide version 8.2) with two metal constraints and default settings. PyMOL³⁸ (Schrödinger; LLC: New York, NY, USA) was used to process each docked pose.

Acknowledgments

This research was supported by the National Institute of Allergy and Infectious Diseases, the National Institutes of Health, United States grant number R01AI136982 (to Robert J. Geraghty and Zhengqiang Wang, USA). We thank the Minnesota Supercomputing Institute for molecular modeling resource and Christine Dreis for technical assistance.

Author contributions

Zhengqiang Wang and Robert J. Geraghty conceptualized the research. Sameera Senaweera and Jayakanth Kankanala designed, synthesized and characterized all compounds. Tiffany Edwards and Yan Wang performed all the biological assays. Rajkumar Lalji Sahani conducted molecular docking. Jiashu Xie performed the ADME assays. Zhengqiang Wang, Sameera Senaweera, Tiffany C. Edwards and Robert J. Geraghty wrote the manuscript. Rajkumar Lalji Sahani and Jiashu Xie edited the manuscript. All authors have read and agreed to the published version of the manuscript.

Conflicts of interest

The authors declare that they have no known competing financial interests or personal relationships that could have appeared to influence the work reported in this paper.

Appendix A. Supporting information

Supporting information to this article can be found online at <https://doi.org/10.1016/j.apsb.2021.08.019>.

References

- Zuhair M, Smit GSA, Wallis G, Jabbar F, Smith C, Devleeschauwer B, et al. Estimation of the worldwide seroprevalence of cytomegalovirus: a systematic review and meta-analysis. *Rev Med Virol* 2019;**29**:e2034.
- Gugliesi F, Coscia A, Griffante G, Galitska G, Pasquero S, Albano C, et al. Where do we stand after decades of studying human cytomegalovirus?. *Microorganisms* 2020;**8**:685.
- Kenneson A, Cannon MJ. Review and meta-analysis of the epidemiology of congenital cytomegalovirus (cmv) infection. *Rev Med Virol* 2007;**17**:253–76.
- Perello R, Vergara A, Monclus E, Jimenez S, Montero M, Saubi N, et al. Cytomegalovirus infection in HIV-infected patients in the era of combination antiretroviral therapy. *BMC Infect Dis* 2019;**19**:1030.
- Gane E, Saliba F, Valdecasas GJ, O'Grady J, Pescovitz MD, Lyman S, et al. Randomised trial of efficacy and safety of oral ganciclovir in the prevention of cytomegalovirus disease in liver-transplant recipients. The oral ganciclovir international transplantation study group [corrected] *Lancet* 1997;**350**:1729–33.
- Britt WJ, Prichard MN. New therapies for human cytomegalovirus infections. *Antivir Res* 2018;**159**:153–74.
- Kimberlin DW, Jester PM, Sanchez PJ, Ahmed A, Arav-Boger R, Michaels MG, et al. Valganciclovir for symptomatic congenital cytomegalovirus disease. *N Engl J Med* 2015;**372**:933–43.
- Kotton CN, Kumar D, Caliendo AM, Huprikar S, Chou S, Danziger-Isakov L, et al. The third international consensus guidelines on the management of cytomegalovirus in solid-organ transplantation. *Transplantation* 2018;**102**:900–31.
- Green ML, Leisenring W, Xie H, Mast TC, Cui Y, Sandmaier BM, et al. Cytomegalovirus viral load and mortality after haemopoietic stem cell transplantation in the era of pre-emptive therapy: a retrospective cohort study. *Lancet Haematol* 2016;**3**:e119–27.
- Chou S. Approach to drug-resistant cytomegalovirus in transplant recipients. *Curr Opin Infect Dis* 2015;**28**:293–9.
- James SH, Prichard MN. The genetic basis of human cytomegalovirus resistance and current trends in antiviral resistance analysis. *Infect Disord - Drug Targets* 2011;**11**:504–13.
- Lurain NS, Chou S. Antiviral drug resistance of human cytomegalovirus. *Clin Microbiol Rev* 2010;**23**:689–712.
- Piret J, Boivin G. Clinical development of letermovir and maribavir: overview of human cytomegalovirus drug resistance. *Antivir Res* 2019;**163**:91–105.
- Goldner T, Hewlett G, Ettischer N, Ruesamen-Schaeff H, Zimmermann H, Lischka P. The novel anticytomegalovirus compound AIC246 (letermovir) inhibits human cytomegalovirus replication through a specific antiviral mechanism that involves the viral terminase. *J Virol* 2011;**85**:10884–93.
- Frietsch JJ, Michel D, Stamminger T, Hunstig F, Birndt S, Schnetzke U, et al. *In vivo* emergence of UL56 C325Y cytomegalovirus resistance to letermovir in a patient with acute myeloid leukemia after hematopoietic cell transplantation. *Mediterr J Hematol Infect Dis* 2019;**11**:e2019001.
- Chou S. Rapid *in vitro* evolution of human cytomegalovirus UL56 mutations that confer letermovir resistance. *Antimicrob Agents Chemother* 2015;**59**:6588–93.
- Gentry BG, Bogner E, Drach JC. Targeting the terminase: an important step forward in the treatment and prophylaxis of human cytomegalovirus infections. *Antivir Res* 2019;**161**:116–24.
- Griffiths PD, Emery VC. Taming the transplantation troll by targeting terminase. *N Engl J Med* 2014;**370**:1844–6.
- Wang Y, Mao L, Kankanala J, Wang Z, Geraghty RJ. Inhibition of human cytomegalovirus pUL89 terminase subunit blocks virus replication and genome cleavage. *J Virol* 2017;**91**:e02152-16.
- Wang Y, Tang J, Wang Z, Geraghty RJ. Metal-chelating 3-hydroxypyrimidine-2,4-diones inhibit human cytomegalovirus pUL89 endonuclease activity and virus replication. *Antivir Res* 2018;**152**:10–7.
- Kankanala J, Wang Y, Geraghty RJ, Wang Z. Hydroxypyridonecarboxylic acids as inhibitors of human cytomegalovirus pUL89 endonuclease. *ChemMedChem* 2018;**13**:1658–63.
- Majorek KA, Dunin-Horkawicz S, Steczkiewicz K, Muszewska A, Nowotny M, Ginalski K, et al. The RNase H-like superfamily: new members, comparative structural analysis and evolutionary classification. *Nucleic Acids Res* 2014;**42**:4160–79.
- Nowotny M. Retroviral integrase superfamily: the structural perspective. *EMBO Rep* 2009;**10**:144–51.
- Bongarzone S, Nadal M, Kaczmarek Z, Machon C, Alvarez M, Albericio F, et al. Structure-driven discovery of alpha,gamma-diketoacid inhibitors against UL89 herpesvirus terminase. *ACS Omega* 2018;**3**:8497–505.
- Kankanala J, Kirby KA, Liu F, Miller L, Nagy E, Wilson DJ, et al. Design, synthesis, and biological evaluations of hydroxypyridonecarboxylic acids as inhibitors of HIV reverse transcriptase associated RNase H. *J Med Chem* 2016;**59**:5051–62.
- Pauwels R, Andries K, Desmyter J, Schols D, Kukla MJ, Breslin HJ, et al. Potent and selective inhibition of HIV-1 replication *in vitro* by a novel series of TIBO derivatives. *Nature* 1990;**343**:470–4.
- Daelemans D, Pauwels R, De Clercq E, Pannecouque C. A time-of-drug addition approach to target identification of antiviral compounds. *Nat Protoc* 2011;**6**:925–33.
- Curatolo W. Physical chemical properties of oral drug candidates in the discovery and exploratory development settings. *Pharmaceut Sci Technol Today* 1998;**1**:387–93.
- Lipinski CA. Drug-like properties and the causes of poor solubility and poor permeability. *J Pharmacol Toxicol* 2000;**44**:235–49.
- Cantrell SR, Bresnahan WA. Interaction between the human cytomegalovirus UL82 gene product (pp71) and hdx regulates immediate-early gene expression and viral replication. *J Virol* 2005;**79**:7792–802.

31. Compton T, Nowlin DM, Cooper NR. Initiation of human cytomegalovirus infection requires initial interaction with cell surface heparan sulfate. *Virology* 1993;**193**:834–41.
32. Chen XX, Murawski A, Patel K, Crespi CL, Balimane PV. A novel design of artificial membrane for improving the pampa model. *Pharm Res-Dordr* 2008;**25**:1511–20.
33. Schrödinger. *Schrödinger small-molecule drug discovery suite 2019-4*. New York, NY, USA: Schrödinger, LLC.; 2019.
34. Schrödinger. *Schrödinger release 2019-4: Maestro*. New York, NY, USA: Schrödinger, LLC.; 2019.
35. Sastry GM, Adzhigirey M, Day T, Annabhimoju R, Sherman W. Protein and ligand preparation: parameters, protocols, and influence on virtual screening enrichments. *J Comput Aided Mol Des* 2013;**27**: 221–34.
36. Jorgensen WL, Maxwell DS, Tirado-Rives J. Development and testing of the OPLS all-atom force field on conformational energetics and properties of organic liquids. *J Am Chem Soc* 1996;**118**: 11225–36.
37. Friesner RA, Murphy RB, Repasky MP, Frye LL, Greenwood JR, Halgren TA, et al. Extra precision glide: docking and scoring incorporating a model of hydrophobic enclosure for protein–ligand complexes. *J Med Chem* 2006;**49**:6177–96.
38. Schrödinger. *The pymol molecular graphics system*. New York, NY, USA: Schrödinger, LLC.; 2019.